Antibacterial and Antifungal Activity of Novel Synthesized Neodymium-Substituted Cobalt Ferrite Nanoparticles for Biomedical Application

Suriya Rehman [1],*, **Mohammad Azam Ansari** [1],*, **Mohammad A. Alzohairy** [2],
Mohammad N. Alomary [3], **B. Rabindran Jermy** [4], **Raheem Shahzad** [5], **Neda Tashkandi** [4]
and Zainab Hassan Alsalem [1]

[1]   Department of Epidemic Disease Research, Institute for Research & Medical Consultations (IRMC), Imam Abdulrahman Bin Faisal University, P.O. Box 1982, Dammam 31441, Saudi Arabia; zhalsalem@iau.edu.sa

[2]   Department of Medical Laboratories, College of Applied Medical Sciences, Qassim University, Qassim 51431, Saudi Arabia; dr.alzohairy@gmail.com

[3]   National Center of Biotechnology, King Abdulaziz City for Science and Technology, Riyadh 11442, Saudi Arabia; malomary@kacst.edu.sa

[4]   Department of Nano-Medicine Research, Institute for Research & Medical Consultations (IRMC), Imam Abdulrahman Bin Faisal University, P.O. Box 1982, Dammam 31441, Saudi Arabia; rJermy@iau.edu.sa (B.R.J.); natashkandi@iau.edu.sa (N.T.)

[5]   Department of Biology, College of Science/Basic and Applied Scientific Research Centre, Imam Abdulrahman Bin Faisal University, P.O. Box 1982, Dammam 31441, Saudi Arabia; rmshahzad@iau.edu.sa

*   Correspondence: surrehman@iau.edu.sa or suriyamir@gmail.com (S.R.); maansari@iau.edu.sa or azammicro@gmail.com (M.A.A.)

Abstract: Neodymium (Nd)-substituted cobalt ferrite nanoparticles (NPs), i.e., $CoNd_xFe_{2-x}O_4$ $(0.0 \leq x \leq 0.2)$ NPs, were synthesized by the sonochemical method. The compositional characterization was done by scanning electron microscopy (SEM) equipped with energy-dispersive X-ray spectroscopy (EDX) and transmission electron microscopy (TEM). Antistaphylococcal activity was found to be enhanced, i.e., survival rate was 50%, 45%, 40%, and 30% with the increase in the ratio of Nd $(0.0 \leq x \leq 0.2)$, whereas anticandidal activity was found efficient, i.e., 9%, 20%, 22%, and 40% survival rate at all the four ratios. The morphogenesis studies indicated that the synthesized metal–ligand, improves the antimicrobial capacity by binding them strongly to the microbial walls. To the best of our knowledge, this is the first report which demonstrates the series of $CoNd_xFe_{2-x}O_4$ $(0.0 \leq x \leq 0.2)$ NPs being active towards *Staphylococcus aureus* and *Candida albicans* and encourages its potential candidature for pharmaceutical and biomedical purposes.

Keywords: neodymium; magnetic nanomaterials; spinel ferrites; antibacterial activity; yeast; bioactivity

1. Introduction

Antimicrobial resistance (AMR), within a vast array of infectious agents, is presently at an alarming stage as a threat to public health around the globe. Foremost attention is being paid to a problem that otherwise may threaten the accomplishments of modern medicine [1]. Penicillin and tetracycline are the most popular and well-documented drugs that may either kill or inhibit the growth of infectious agents [2]. However, the developing resistance of microbes to these and other antimicrobials has led to extensive research to design novel materials [3]. Metal and metal oxide nanoparticles (NPs) are one of the most attractive fields for superior and target specific activity against the resistant microbes [4,5]. Among these, nanocrystalline ferrites have been extensively studied for

nearly a decade owing to their rare structural, electrical, and magnetic properties. Ferrite NPs have promising applications in numerous biomedical fields, such as magnetic hyperthermia, magnetically guided drug delivery, magnetic resonance imaging, and as antimicrobials [6–8]. Antimicrobial activity of such particles is attributed to the cation attraction of the microbial protein material, which gets precipitated as an insoluble proteinate leading to cell death. Hg^{2+}, Co^{2+}, Cu^{2+}, and Pb^{2+} have been reported to possess antimicrobial activities, but are simultaneously toxic to human cells, hence not suitable for treating infectious diseases [9]. Nonetheless, a few strategies have been devised to overcome such toxicity. One way is the utilization of a fine covering entity over these particles, and the other is to prepare the metal complexes without a change in the activity they possess, making them non-toxic. Successful reports on various biocompatible agents, such as citrate, dextrin, polystyrene, gold, silver, and zinc, have been studied for biomedical and antimicrobial utilization [10–12]. Therefore, the properties of ferrites can be enhanced by conjugated metallic ions in their structure, such as cobalt and iron ions [13]. Interestingly, the substitution of spinel ferrites by rare earth elements (RE) has been reported to modulate the magnetic behavior, coercivity, and grain size attractive for magneto–optical applications [14]. Avazpour et al. [15] reported that cobalt ferrite substituted by rare earth, such as neodymium and europium, tends to inhibit crystallite size (grain growth) between 11 and 31 nm and enhance the coercivities (~2 kOe coercive field). The effect of cobalt ferrites substituted by neodymium (Nd^{3+}), samarium (Sm^{3+}), and gadolinium (Gd^{3+}) on magnetic, crystal size, and Curie temperature were reported by Nikumbh et al. [16].

Cobalt ferrite has been an interesting field in the past few decades for its unique and controllable characteristics and its potential use in biomedical applications, such as enhanced drug stability/solubility, and reduced side effects [17–21], Amiri and Shokrollahi, 2013, Hathout et al., 2017. Metal combination with cobalt ferrite could obtain new complex materials with improved bioactivity, and such experiments on the antimicrobial aspect of ferrites have achieved success [22,23]. Copper and cobalt substituted cobalt ferrite was reported to influence the microstructure of ferrite nanoparticles (40–50 nm) and exhibit antibacterial activity [8,24,25], Sanpo et al., 2013, Samavati and Ismail, 2017, Maksoud et al., 2019, Ashour et al., 2018. *Staphylococcus aureus* and *Escherichia coli* are two of the notorious and the most clinically relevant bacteria known for developing resistance to many commonly used antimicrobials. Infections caused by these antibiotic-resistant strains have attained an epidemic extent worldwide for which the treatment has become a challenge [26,27]. Among the fungal pathogen, *Candida albicans* is the most prevalent forms, possessing a biofilm-producing ability on both biological and other surfaces. Additionally, pathogenicity mediated by biofilms on devices such as artificial prosthesis, dentures, pacemakers, prosthetic joints, central venous catheter, intrauterine device, etc., display a calamitous effect [12].

2. Materials and Methods

2.1. Synthesis of CoNd$_x$Fe$_{2-x}$O$_4$ (0.0 ≤ x ≤ 0.2) NPs

The series of CoNd$_x$Fe$_{2-x}$O$_4$ (0.0 ≤ x ≤ 0.2) NPs were synthesized by the sonochemical approach. Analytical grade cobalt nitrate (Co(NO$_3$)$_2$•6H$_2$O), iron nitrate (Fe(NO$_3$)$_3$•9H$_2$O), and Neodymium(III) nitrate hexahydrate (Nd(NO$_3$)$_3$•6H$_2$O) were chosen as source material for Co, Fe, and Nd, respectively. An aqueous solution of starting precursors (Co, Fe, and Nd) in their stoichiometric ratio was prepared by dissolving in deionized water. An aqueous solution of NaOH (3 M) was mixed with the above-prepared nitrate solution by constant stirring using magnetic stirrer. Further, the mixed solution was exposed to high-intensity ultrasonic irradiation (frequency: 20 kHz and power: 70 W) (Ultrasonic homogenizer UZ SONOPULS HD 2070, Bandelin, Berlin, Germany) for 60 min. After 60 min of ultrasonic irradiation, the reaction temperature was 90 °C. The prepared NPs were separated by a centrifuge process at 4000 rpm for 30 min. The obtained NPs were washed several times in deionized water for the complete removal of sodium ions. Then, the obtained washed NPs were dried at 60 °C for 24 h [28].

2.2. Instrumentation

Phase identification was executed by a Rigaku Benchtop Miniflex powder X-ray diffraction (XRD) analyzer with Cu Kα radiation at room temperature (RT: 20–70 °C). The morphological, elemental, and microstructural analyses of the products were analyzed by field emission scanning electron microscopy (JSM-7610F, Tokyo, Japan) and (scanning) transmission electron microscopy (TEM/STEM, FEI Titan G2, Hillsboro, OR, USA) equipped with energy-dispersive X-ray spectroscopy (EDX). The samples analyzed by TEM were prepared by dropping particle dispersions onto carbon-coated Cu grids and air-dried before mounting onto the microscope. Fourier-transform infrared spectra (FTIR, Bruker) were recorded using a spectrometer over a range of 4000 to 400 cm^{-1}. Further, the mixed solution was exposed to high-intensity ultrasonic irradiation (frequency: 20 kHz and power: 70 W) (Ultrasonic homogenizer UZ SONOPULS HD 2070).

2.3. Determination of Antibacterial and Anti-Yeast Activity

Preparation of Inoculum

Synthesized neodymium (Nd) cobalt NPs, i.e., $CoNd_xFe_{2-x}O_4$ (0.0 ≤ x ≤ 0.2), were subjected to Gram-positive *Staphylococcus aureus* subsp. *aureus* Rosenbach (ATCC® 25923™), Gram-negative bacteria *Escherichia coli* (ATCC® 35218™), and *Candida albicans* (ATCC® 14053) as yeast. The inoculum was prepared by inoculating a freshly prepared single colony of bacteria and the yeast into Mueller Hinton Broth (MHB) and Sabauraud Broth (SDB), respectively. The cultures were incubated for 18 h at 37 ± 2 °C and 28 ± 2 °C for 48 h, respectively. After incubation, washing of harvested culture was done with phosphate-buffered saline (PBS), and the cell density of cell suspension was adjusted to approximately 10^7 CFU/mL by diluting with sterile MHB/SDB, respectively.

2.4. Evaluation of Growth Pattern in the Presence of Nanomaterial

Several test concentrations of synthesized NPs were applied to cell cultures for the initial screening study. After the initial screening, 1 mg/mL was selected for further studies. Briefly, sterile tubes containing 1 mg/mL of NPs in sterile water were subjected to sonication for 25 min to avoid the formation of NPs aggregates. Then, they were added to the suitable growth media of each organism. To prevent bottom settlement and clumping of the NPs during incubation, the prepared cell suspension with NPs were incubated in a rotary shaker at 150 rpm for 18 h at 37 ± 2 °C, and 48 h at 28 ± 2 °C for bacteria and yeast, respectively. The growth of each organism was evaluated by measuring optical density (OD) at 600 nm by spectrophotometer (UV-BT-610, Brite technologies INC., BC, Canada). Control experiments were also run in parallel. A growth medium with nanomaterials was used as a negative control, and culture medium without nanomaterials was taken as growth control. To evaluate the growth pattern of the organism in the presence of test nanomaterial, the OD was recorded at every 3, 6, and 18 h for the bacteria, and 24 and 48 h for the yeast. The obtained values for OD of controls were subtracted from the culture media with NPs [29].

2.5. Determination of Colony Forming Units

For evaluating the effectiveness of a test nanomaterial, it is important to determine the viable microbial cell concentrations by counting colony-forming units (CFU), and number of live bacteria in a sample after treating with the test materials. This was performed by plating them on a suitable growth media. One hundred microliters of NPs-treated culture was spread aseptically onto a suitable agar plate. After the incubation period was over, the number of colonies on a plate were counted. Each colony counted was considered to have originated from a single viable microbial cell. The rate of survival percentage of the organisms was determined by using the formula, S% = (A/B) × 100 (where, A is the number of CFU in the medium treated with nanomaterial, and B is the number of CFU in the control).

2.6. Study of Morphogenesis of the Treated Microbes

The effect of synthesized NPs on the morphogenesis of treated microbial cells was further analyzed by scanning electron microscopy (SEM). Precisely, 10^6 CFU/mL of *S. aureus* and *C. albicans* were subjected to 1 mg/mL of NPs at 18 h at $37 \pm 2\,°C$ and $28 \pm 2\,°C$ at 48 h, respectively. As a note, *E. coli* was excluded due to its minimum activity found at both broth and agar cultures. Treated cells were centrifuged and washed three to four times with PBS. Two-point five percent glutaraldehyde was used for the primary fixation and subsequent fixation with 1% osmium tetroxide. The fixation of samples was achieved by washing and dehydration with varying concentrations of ethanol. The prepared samples were placed on the stubs, left for drying using a desiccator, and finally coated with gold. Coated samples were analyzed at an accelerating voltage of 20 kV by SEM [30,31].

3. Results and Discussion

3.1. Structural and Morphological Analysis along with EDX and Elemental Mapping

Figure 1 displays the X-ray powder pattern of $CoNd_xFe_{2-x}O_4$ ($0.0 \leq x \leq 0.2$) NPs. All the compositions exhibited the indexed peaks of Co spinel ferrite without the presence of any secondary phase. This would afford the formation of pure, high-quality, and well substituted Nd^{3+} into the $CoFe_2O_4$ structure. Rietveld refinement is employed to estimate the lattice parameters and crystal size. It was found that the lattice parameters "a" increased with the increasing Nd ratios. This is due to the difference in the ionic radii between Fe^{3+} (0.645 Å) and Nd^{3+} (0.98 Å), which leads to enlarging the lattice. In addition, it is noticed that the average crystallite size is in the range of 9 to 16 nm. The FE-SEM (Field Emission Scanning Electron Microscopy) images of $CoNd_xFe_{2-x}O_4$ ($x = 0.0$, 0.1, and 0.2) NPs are presented in Figure 2A. The images show the aggregation of spherical particles with uniform distribution. The TEM images of (i) $CoFe_2O_4$ ($x = 0.0$) and (ii) $CoNd_{0.2}Fe_{1.8}O_4$ ($x = 0.2$) NPs are presented in Figure 2B. Agglomeration of NPs was also observed, owing to the magnetic nature of the product (Figure 2B). About 15 nm average particle size was estimated from these TEM images. The EDX and elemental mapping of $CoNd_xFe_{2-x}O_4$ ($x = 0.0$, 0.1 and 0.2) are recorded in Figure 3. The spectrum revealed the quantification of consistent elements that occurred in $CoNd_xFe2_{-x}O_4$ ($x = 0.0$, 0.1, and 0.2). The results confirmed that the sonochemical approach is the best, easy, and cost-effective technique for achieving homogenies (pure) spinel ferrites.
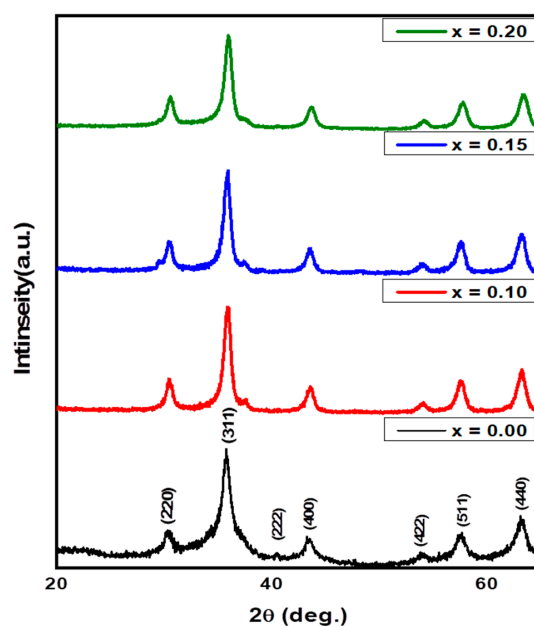
Figure 1. XRD powder patterns of $CoNd_xFe_{2-x}O_4$ ($0.0 \leq x \leq 0.2$) nanoparticles (NPs).
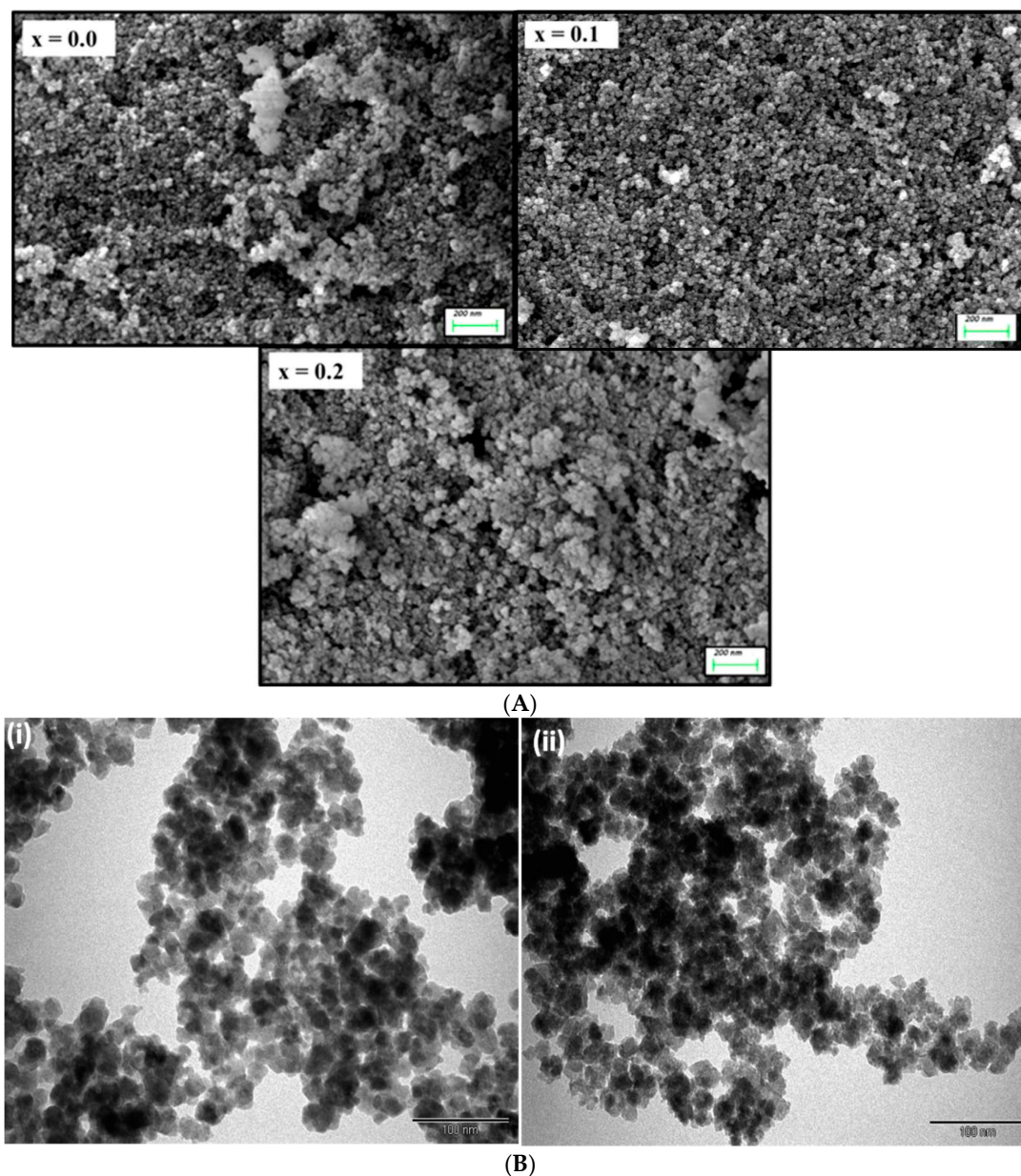
Figure 2. (**A**) FE-SEM of CoNd$_x$Fe$_{2-x}$O$_4$ (0.0 ≤ x ≤ 0.2) NPs; (**B**) TEM images of (i) CoFe$_2$O$_4$ (x = 0.0), (ii) CoNd$_{0.2}$Fe$_{1.8}$O$_4$ (x = 0.2) NPs.

In the present study, the antibacterial and anticandidal efficacy of CoNd$_x$Fe$_{2-x}$O$_4$ (0.0 ≤ x ≤ 0.2) was determined using both broth and agar-based growth cultures. The nanomaterials were treated at a concentration of 1 mg/mL. The OD and examination of the viable count of the bacteria and yeast in the inoculated media were investigated as the activity of the content of Nd. After determining the OD of *S. aureus* and *E. coli* for 3, 6, and 18 h incubation, and *C. albicans* for 24 and 48 h, it was observed that the growth of *S. aureus* was reduced with sample x = 0.15 and x = 0.2 as compared to sample x = 0.0 and x = 0.1, while *E. coli* was found to have growth pattern similar to control (untreated *E. coli*) with only a slight variation with x = 0.0. However, *C. albicans* growth was found to inhibited by all the four ratios with profound inhibition when treated with the least Nd, i.e., x = 0.0 and x = 0.1 (Figure 4).
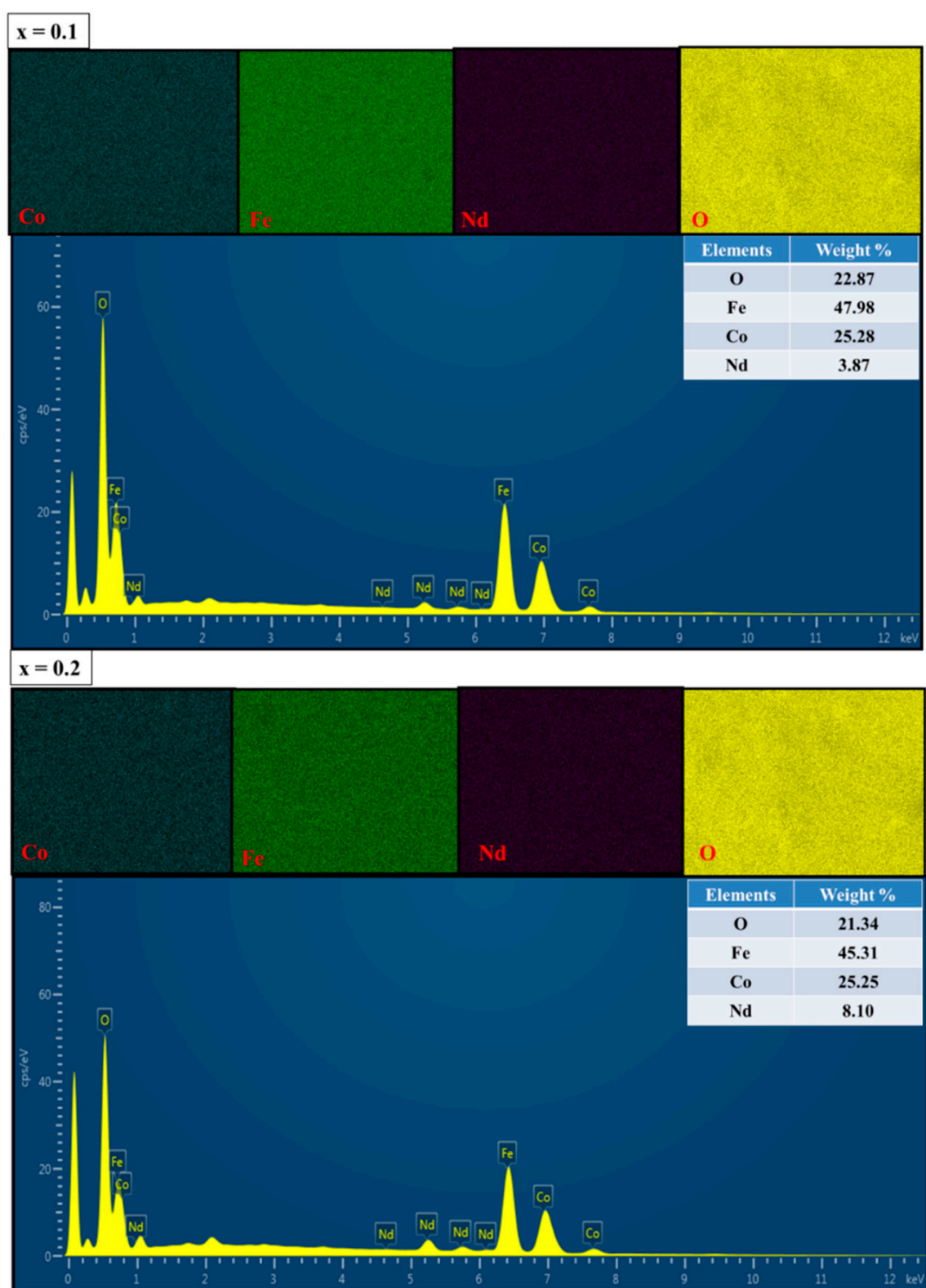
Figure 3. EDX spectra of $CoNd_xFe_{2-x}O_4$ ($0.0 \leq x \leq 0.2$) NPs.
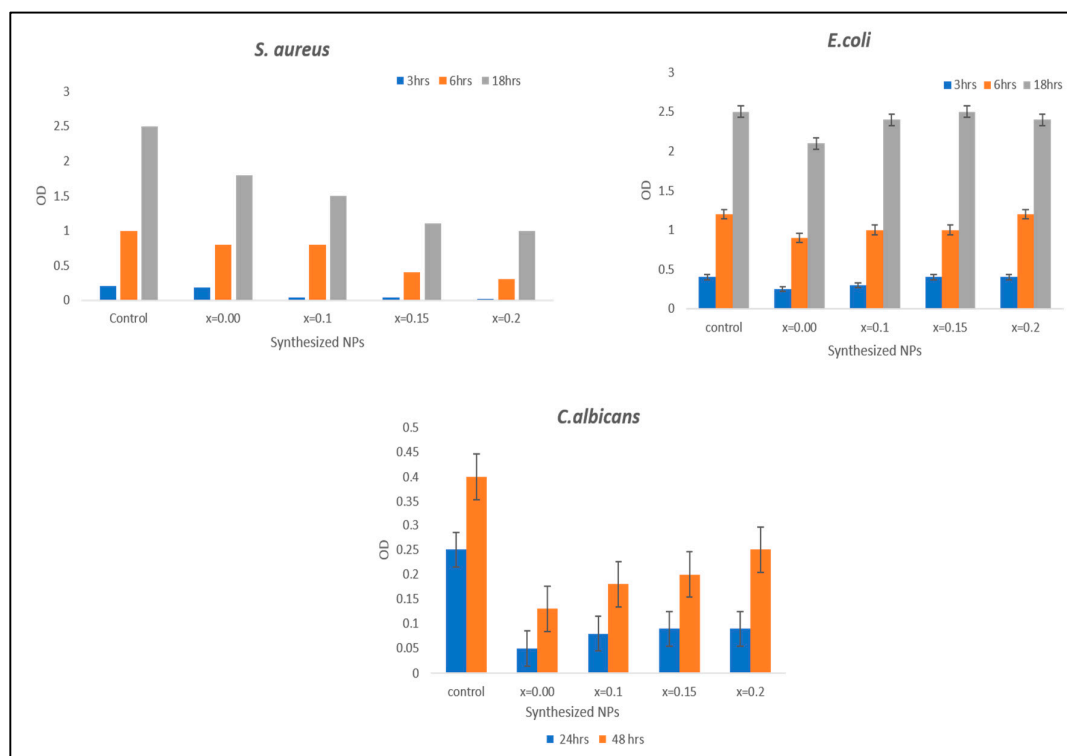
Figure 4. Growth pattern of microbes treated with 1 mg/mL of $CoNd_xFe_{2-x}O_4$ ($0.0 \leq x \leq 0.2$) NPs at different time intervals, control; untreated cells.

The survival rate of test organisms was calculated as per the formula mentioned above and was expressed in percentage. Colonies of *S. aureus* and *E. coli* were counted after 18 h of incubation, and *C. albicans* after 48 h. The viable cell count of the test organisms demonstrated that the number of viable *S. aureus* and *C. albicans* was rationally less than the control (Figure 5A). All the four ratios had a profound effect on the survival of *S. aureus* in both experiments, with the least survival rate of 50%, 45%, 40%, and 30% found with the increased ratio of Nd in the x = 0.0, x = 0.1, x = 0.15, and x = 0.2, respectively. *E. coli* was found to have a negligible effect of all the four ratios, with only x = 0.0 having 90% survival. However, extraordinary activity was seen with profound inhibition in the growth of *C. albicans* having 9%, 20%, 22%, and 40% survival at the given concentration of all four ratios, respectively, with a slightly better inhibition with x = 0.0 and x = 0.1 (Figure 5B).

Recently, a study by Ashour et al. [25] demonstrated that metal substituted cobalt ferrite NPs, such as copper–cobalt ferrite, zinc–cobalt ferrite, and manganese–cobalt ferrite, inhibit the growth of bacteria and yeast. However, to the best of our knowledge, this is the first report of Nd substituted cobalt NPs with broad-spectrum antimicrobial activity against gram-positive/negative bacterium and yeast. It was found in our study that, as the dopant content, i.e., when Nd increases from 0.0 to 0.2, the anti-gram-positive bacterium activity of NPs was also increased, although anti-gram-negative bacterium activity was found negligible which is in agreement with the studies conducted by Ashour et al., 2018. It is of paramount importance to mention that antibacterial studies conducted by Ishaq et al. [32] using nickel ferrite NPs also found no activity against *E. coli* and showed activity only against *S. aureus.* This specificity of action could be attributed to the difference in the cell wall thickness and the amount of lipopolysaccharide content among gram-positive and gram-negative bacteria [33].
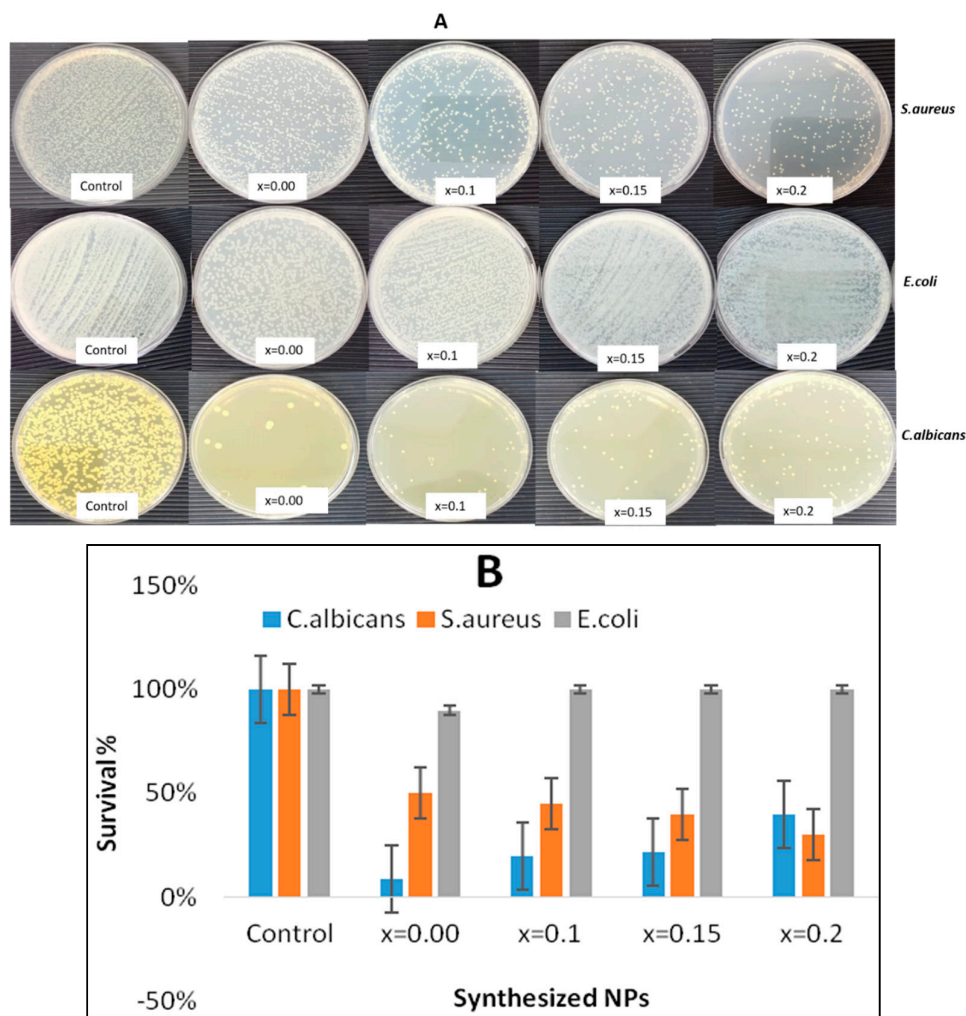
Figure 5. (**A**) Culture plates and (**B**) Survival rate (%), of treated microbes with 1 mg/mL of $CoNd_xFe_{2-x}O_4$ ($0.0 \leq x \leq 0.2$) NPs, Control; untreated cells.

The present study also demonstrated that the anticandidal activity of synthesized NPs was extra ordinary. However, with the increase in the content of Nd, a slight decline in the anticandidal activity was observed. Further, we observed that the NPs inhibit microbial growth in a size-dependent manner indicating small size NPs exhibit strong anticandidal activity, and increased Nd inhibit bacterial growth.

The absence of growth in the presence of NPs is an indirect detection of the ability of the NPs to kill or inhibit the growth. The activity could be due to the small size and the surface area of the particles. An increase in surface area increases the number of atoms on the surface, which leads to an increase in the biological activity. It is suggested that the NPs exhibit particle size-dependent antimicrobial activity. The reduced size permits the particles to penetrate the cell wall of the microbial cells, rupturing the cytoplasmic membrane, which leads to cell death. Additionally, the dispersion of NPs in aqueous solution is also an important aspect of the antimicrobial action, which increases with a decrease in particle size [34–37]. As a result, the enhanced activity of the nanomaterial with increasing Nd content could possibly be due to the surface to volume ratio, offering better contact with the bacterial cell.

3.2. Determination of Morphogenesis of Treated Cells

The morphogenesis caused by $CoNd_xFe_{2-x}O_4$ ($0.0 \leq x \leq 0.2$) on *S. aureus* cells and *C. albicans* were also studied by scanning electron microscopy (SEM) analysis. The control (i.e., untreated) *S. aureus* cells were a normal spherical shape with a smooth cell surface. Treated *S. aureus* with x = 0.0 and x = 0.1 NPs showed significant damage, however, when treated with x = 0.15 and x = 0.2, the *S. aureus* cells were

found not only severely damaged but also with a significant reduction in number. The non-intact cells were found to have distorted and deformed cell walls and cytoplasmic membranes, which indicates loss of membrane integrity and hence, a potential cause of cell death (Figure 6A).

Similarly, the untreated *C. albicans* cells were normal in morphology with smooth cell walls and membranes, while as all the four ratios of Nd, NPs had a devastating effect on the *C. albicans* cell morphogenesis. When treated with x = 0.0 and x = 0.1 NPs, the count of *C. albicans* cells dramatically decreased, and the critically affected cells were no longer intact, which may ultimately cause cell death (Figure 6B).

As evident from the SEM micrographs, significant damage to *S. aureus* and *C. albicans* cells were observed. The NP treatment of the cells may cause membrane damage due to NPs adsorption and penetration into the cell. Studies suggest that the primary mode of action is the loss of membrane integrity due to adsorption. Adsorption of NPs also causes the cell wall to depolarize, which alters the negative charge of the cell surface to become more permeable [33]. It has been reported the dual-action may take place, and the cell wall is damaged, leading to penetration of NPs [38]. Alternately, reactive oxygen species (ROS) are produced that prevent DNA replication. The production of ROS may play a part in the primary step, as well [39]. Recently, it was reported by Scheres and Krom 2016, that *C. albicans* and *S. aureus* can coexist in polymicrobial biofilms, which may cause more severe and widespread infection than either of them alone. Hence, the obtained results of $CoNd_xFe_{2-x}O_4$ $(0.0 \leq x \leq 0.2)$ NPs in our study offer a possible solution to such co-existing infectious agents [40].
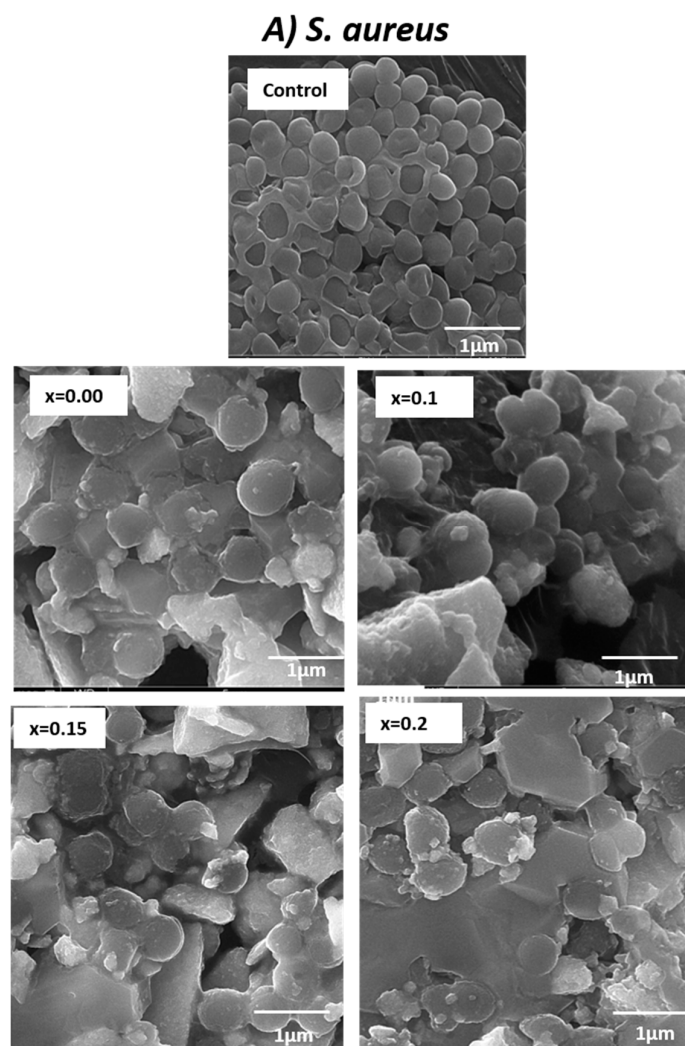
Figure 6. *Cont.*
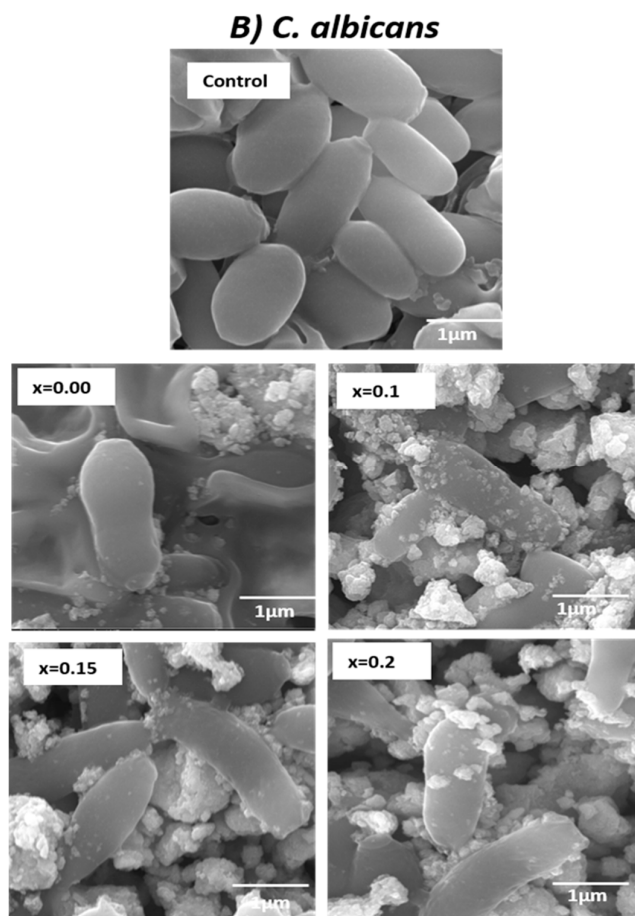
Figure 6. (**A**) SEM images for the morphogenesis of treated *S. aureus* with 1 mg/mL of $CoNd_xFe_{2-x}O_4$ ($0.0 \leq x \leq 0.2$) NPs; (**B**) SEM images for the morphogenesis of treated *C. albicans* with 1 mg/mL of $CoNd_xFe_{2-x}O_4$ ($0.0 \leq x \leq 0.2$) NPs.

4. Conclusions

Sonochemical synthesis of Nd substituted cobalt ferrite nanoparticles, i.e., $CoNd_xFe_{2-x}O_4$ ($0.0 \leq x \leq 0.2$) NPs, has been successfully achieved in the present study. Furthermore, with a focus on the applied part of synthesized nanomaterials, the antibacterial and anticandidal efficacy was tested against *S. aureus*, *E. coli*, and *C. albicans.* The obtained results showed an enhancement in the bactericidal activity with the addition of Nd into cobalt ferrite, unlike anticandidal activity, which was profound with all the four ratios. The enhanced activity is attributed to the varying ratios of Nd, which in turn offered an increase in the ratio of surface to volume of nanoparticles resulting in improved interaction with the microbes. Therefore, the Nd substituted cobalt ferrite nanoparticles having good magnetic and antimicrobial activities, which hold great potential in pharmaceutical and biomedical applications.

Data Availability: The data used to support the findings of this study are included within the article.

Author Contributions: Conceptualization, S.R., M.A.A. (Mohammad Azam Ansari); Methodology, Z.H.A., N.T.; Software, B.R.J., R.S.; Validation and Formal Analysis, M.A.A. (Mohammad A. Alzohairy), M.N.A.; Investigation, S.R., M.A.A. (Mohammad Azam Ansari); Writing—Original Draft Preparation, S.R., Writing—Review & Editing, S.R., M.A.A. (Mohammad Azam Ansari) and B.R.J.

Funding: This research received no external funding.

Acknowledgments: The authors gratefully acknowledge Abdulhadi Baykal and Munerah Abdullah Almessiere, Institute for Research & Medical Consultations (IRMC), Imam Abdulrahman Bin Faisal University (IAU-Saudi Arabia) for supervising and supporting this study.

Conflicts of Interest: The authors declare no conflict of interest.

References

1. Organization WH. *Antimicrobial Resistance: Global Report on Surveillance*; World Health Organization: Geneva, Switzerland, 2014.
2. Falagas, M.E.; Karageorgopoulos, D.E. Pandrug resistance (PDR), extensive drug resistance (XDR), and multidrug resistance (MDR) among Gram-negative bacilli: Need for international harmonization in terminology. *Clin. Infect. Dis.* **2008**, *46*, 1121–1122. [CrossRef] [PubMed]
3. Levy, S.B. *Balancing the Drug-Resistance Equation*; Elsevier Current Trends: Amsterdam, The Netherlands, 1994.
4. El-Batal, A.I.; El-Sayyad, G.S.; El-Ghamery, A.; Gobara, M. Response surface methodology optimization of melanin production by Streptomyces cyaneus and synthesis of copper oxide nanoparticles using gamma radiation. *J. Clust. Sci.* **2017**, *28*, 1083–1112. [CrossRef]
5. Žalnėravičius, R.; Paškevičius, A.; Kurtinaitiene, M.; Jagminas, A. Size-dependent antimicrobial properties of the cobalt ferrite nanoparticles. *J. Nanopart. Res.* **2016**, *18*, 300. [CrossRef]
6. Goldman, A. *Modern Ferrite Technology*; Springer Science & Business Media: Berlin, Germany, 2006.
7. Hutmacher, D.W.; Schantz, J.T.; Lam, C.X.F.; Tan, K.C.; Lim, T.C. State of the art and future directions of scaffold-based bone engineering from a biomaterials perspective. *J. Tissue Eng. Regen. Med.* **2007**, *1*, 245–260. [CrossRef]
8. Sanpo, N.; Berndt, C.C.; Wen, C.; Wang, J. Transition metal-substituted cobalt ferrite nanoparticles for biomedical applications. *Acta Biomater.* **2013**, *9*, 5830–5837. [CrossRef]
9. Hatamie, S.; Nouri, M.; Karandikar, S.; Kulkarni, A.; Dhole, S.; Phase, D.; Kale, S.N. Complexes of cobalt nanoparticles and polyfunctional curcumin as antimicrobial agents. *Mater. Sci. Eng. C* **2012**, *32*, 92–97. [CrossRef]
10. Cunningham, C.H.; Arai, T.; Yang, P.C.; McConnell, M.V.; Pauly, J.M.; Conolly, S.M. Positive contrast magnetic resonance imaging of cells labeled with magnetic nanoparticles. *Magn. Reson. Med Off. J. Int. Soc. Magn. Reson. Med.* **2005**, *53*, 999–1005. [CrossRef]
11. Lu, C.-W.; Hung, Y.; Hsiao, J.-K.; Yao, M.; Chung, T.-H.; Lin, Y.-S.; Wu, S.H.; Hsu, S.C.; Liu, H.M.; Mou, C.Y.; et al. Bifunctional magnetic silica nanoparticles for highly efficient human stem cell labeling. *Nano Lett.* **2007**, *7*, 149–154. [CrossRef]
12. Sharma, R.P.; Raut, S.D.; Jadhav, V.V.; Kadam, A.S.; Mane, R.S. Anti-candida and anti-adhesion efficiencies of zinc ferrite nanoparticles. *Mater. Lett.* **2019**, *237*, 165–167. [CrossRef]
13. Ghafoor, A.; Khan, M.A.; Islam, M.; Gilani, Z.A.; Manzoor, A.; Khan, H.M.; Ali, I.; Warsi, M.F. Structural and electromagnetic studies of $Ni_{0.7}Zn_{0.3}HO_{2x}Fe_{2-2x}O_4$ ferrites. *Ceram. Int.* **2016**, *42*, 14252–14256. [CrossRef]
14. Routray, K.L.; Saha, S.; Sanyal, D.; Behera, D. Role of rare-earth (Nd^{3+}) ions on structural, dielectric, magnetic and Mossbauer properties of nano-sized $CoFe_2O_4$: Useful for high frequency application. *Mater. Res. Express* **2018**, *6*, 026107. [CrossRef]
15. Avazpour, L.; Shokrollahi, H.; Toroghinejad, M.R.; Khajeh, M.Z. Effect of rare earth substitution on magnetic and structural properties of $Co_{1-x}RE_x Fe_2O_4$ (RE: Nd, Eu) nanoparticles prepared via EDTA/EG assisted sol–gel synthesis. *J. Alloy. Compd.* **2016**, *662*, 441–447. [CrossRef]
16. Nikumbh, A.K.; Pawar, R.A.; Nighot, D.V.; Gugale, G.S.; Sangale, M.D.; Khanvilkar, M.B.; Nagawade, A.V. Structural, electrical, magnetic and dielectric properties of rare-earth substituted cobalt ferrites nanoparticles synthesized by the co-precipitation method. *J. Magn. Magn. Mater.* **2014**, *355*, 201–209. [CrossRef]
17. Tatarchuk, T.; Bououdina, M.; Paliychuk, N.; Yaremiy, I.; Moklyak, V. Structural characterization and antistructure modeling of cobalt-substituted zinc ferrites. *J. Alloy. Compd.* **2017**, *694*, 777–791. [CrossRef]
18. Gupta, A.K.; Gupta, M. Synthesis and surface engineering of iron oxide nanoparticles for biomedical applications. *Biomaterials* **2005**, *26*, 3995–4021. [CrossRef]
19. Pankhurst, Q.; Thanh, N.; Jones, S.; Dobson, J. Progress in applications of magnetic nanoparticles in biomedicine. *J. Phys. D Appl. Phys.* **2009**, *42*, 224001. [CrossRef]
20. Amiri, S.; Shokrollahi, H. The role of cobalt ferrite magnetic nanoparticles in medical science. *Mater. Sci. Eng. C* **2013**, *33*, 1–8. [CrossRef]

21. Hathout, A.S.; Aljawish, A.; Sabry, B.A.; El-Nekeety, A.A.; Roby, M.H.; Deraz, N.M.; Aly, S.E.; Abdel-Wahhab, M.A. Synthesis and characterization of cobalt ferrites nanoparticles with cytotoxic and antimicrobial properties. *J. Appl. Pharm. Sci.* **2017**, *7*, 086–092. [CrossRef]

22. Samavati, A.; Ismail, A. Antibacterial properties of copper-substituted cobalt ferrite nanoparticles synthesized by co-precipitation method. *Particuology* **2017**, *30*, 158–163. [CrossRef]

23. Elayakumar, K.; Dinesh, A.; Manikandan, A.; Palanivelu, M.; Kavitha, G.; Prakash, S.; Kumar, R.T.; Jaganathan, S.K.; Baykal, A. Structural, morphological, enhanced magnetic properties and antibacterial bio-medical activity of rare earth element (REE) Cerium (Ce^{3+}) doped $CoFe_2O_4$ nanoparticles. *J. Magn. Magn. Mater.* **2018**, *476*, 157–165. [CrossRef]

24. Maksoud, M.A.; El-Sayyad, G.S.; Ashour, A.H.; El-Batal, A.I.; Elsayed, M.A.; Gobara, M.; El-Khawaga, A.M.; Abdel-Khalek, E.K.; El-Okr, M.M. Antibacterial, antibiofilm, and photocatalytic activities of metals-substituted spinel cobalt ferrite nanoparticles. *Microb. Pathog.* **2019**, *127*, 144–158. [CrossRef] [PubMed]

25. Ashour, A.H.; El-Batal, A.I.; Maksoud, M.A.; El-Sayyad, G.S.; Labib, S.; Abdeltwab, E.; El-Okr, M.M. Antimicrobial activity of metal-substituted cobalt ferrite nanoparticles synthesized by sol–gel technique. *Particuology* **2018**, *40*, 141–151. [CrossRef]

26. Deyno, S.; Toma, A.; Worku, M.; Bekele, M. Antimicrobial resistance profile of staphylococcus aureus isolates isolated from ear discharges of patients at University of Hawassa comprehensive specialized hospital. *BMC Pharmacol. Toxicol.* **2017**, *18*, 35. [CrossRef] [PubMed]

27. Morrill, H.J.; Morton, J.B.; Caffrey, A.R.; Jiang, L.; Dosa, D.; Mermel, L.A.; LaPlante, K.L. Antimicrobial resistance of Escherichia coli urinary isolates in the Veterans Affairs Healthcare System. *Antimicrob. Agents Chemother.* **2017**, *61*, e02236-16. [CrossRef] [PubMed]

28. Yadav, R.S.; Kuřitka, I.; Vilcakova, J.; Havlica, J.; Kalina, L.; Urbánek, P.; Machovsky, M.; Skoda, D.; Masař, M.; Holek, M. Sonochemical synthesis of Gd^{3+} doped $CoFe_2O_4$ spinel ferrite nanoparticles and its physical properties. *Ultrason. Sonochem.* **2018**, *40*, 773–783. [CrossRef] [PubMed]

29. Tank, K.P.; Chudasama, K.S.; Thaker, V.S.; Joshi, M.J. Cobalt-doped nanohydroxyapatite: Synthesis, characterization, antimicrobial and hemolytic studies. *J. Nanopart. Res.* **2013**, *15*, 1644. [CrossRef]

30. Jalal, M.; Ansari, M.A.; Ali, S.G.; Khan, H.M.; Rehman, S. Anticandidal activity of bioinspired ZnO NPs: Effect on growth, cell morphology and key virulence attributes of Candida species. *Artif. Cells Nanomed. Biotechnol.* **2018**, *46*, 912–925. [CrossRef]

31. Rehman, S.; Jermy, B.R.; Akhtar, S.; Borgio, J.F.; Abdul Azeez, S.; Ravinayagam, V.; Al Jindan, R.; Alsalem, Z.H.; Buhameid, A.; Gani, A. Isolation and characterization of a novel thermophile; Bacillus haynesii, applied for the green synthesis of ZnO nanoparticles. *Artif. Cells Nanomed. Biotechnol.* **2019**, *47*, 2072–2082. [CrossRef]

32. Ishaq, K.; Saka, A.A.; Kamardeen, A.O.; Ahmed, A.; Alhassan MIh Abdullahi, H. Characterization and antibacterial activity of nickel ferrite doped α-alumina nanoparticle. *Eng. Sci. Technol. Int. J.* **2017**, *20*, 563–569. [CrossRef]

33. Stoimenov, P.K.; Klinger, R.L.; Marchin, G.L.; Klabunde, K.J. Metal oxide nanoparticles as bactericidal agents. *Langmuir* **2002**, *18*, 6679–6686. [CrossRef]

34. Raghupathi, K.R.; Koodali, R.T.; Manna, A.C. Size-dependent bacterial growth inhibition and mechanism of antibacterial activity of zinc oxide nanoparticles. *Langmuir* **2011**, *27*, 4020–4028. [CrossRef] [PubMed]

35. Sharma, N.; Kumar, J.; Thakur, S.; Sharma, S.; Shrivastava, V. Antibacterial study of silver doped zinc oxide nanoparticles against Staphylococcus aureus and Bacillus subtilis. *Drug Invent. Today* **2013**, *5*, 50–54. [CrossRef]

36. Gingasu, D.; Mindru, I.; Patron, L.; Calderon-Moreno, J.M.; Mocioiu, O.C.; Preda, S.; Stanica, N.; Nita, S.; Dobre, N.; Popa, M.; et al. Green synthesis methods of $CoFe_2O_4$ and $Ag-CoFe_2O_4$ nanoparticles using hibiscus extracts and their antimicrobial potential. *J. Nanomater.* **2016**, *2016*. [CrossRef]

37. Ansari, M.A.; Baykal, A.; Asiri, S.; Rehman, S. Synthesis and characterization of antibacterial activity of spinel chromium-substituted copper ferrite nanoparticles for biomedical application. *J. Inorg. Organomet. Polym. Mater.* **2018**, *28*, 2316–2327. [CrossRef]

38. Ansari, M.A.; Alzohairy, M.A. One-pot facile green synthesis of silver nanoparticles using seed extract of phoenix dactylifera and their bactericidal potential against MRSA. *Evid. Based Complement. Altern. Med.* **2018**. [CrossRef]

39. Simon-Deckers, A.; Loo, S.; Mayne-L'hermite, M.; Herlin-Boime, N.; Menguy, N.; Reynaud, C.; Gouget, B.; Carriere, M. Size-, composition-and shape-dependent toxicological impact of metal oxide nanoparticles and carbon nanotubes toward bacteria. *Environ. Sci. Technol.* **2009**, *43*, 8423–8429. [CrossRef]

40. Scheres, N.; Krom, B.P. Staphylococcus–Candida Interaction Models: Antibiotic Resistance Testing and Host Interactions. In *Candida Species: Methods and Protocols*; Calderone, R., Cihlar, R., Eds.; Springer: New York, NY, USA, 2016; pp. 153–161.